Supporting Information for:

Does Ozone-Water Complex Produce Additional OH Radicals in the Atmosphere?

Bing Jin,[1] Man-Nung Su,[1] and Jim Jr-Min Lin[1,2,3*]

[1]Institute of Atomic and Molecular Sciences, Academia Sinica, Taipei, Taiwan 10617

[2]Department of Chemistry, National Taiwan University, Taipei, Taiwan 10617

[3]Department of Applied Chemistry, National Chiao Tung University, Hsinchu, Taiwan 30010

*To whom correspondence should be addressed. E-mail: jimlin@gate.sinica.edu.tw

I. Experimental

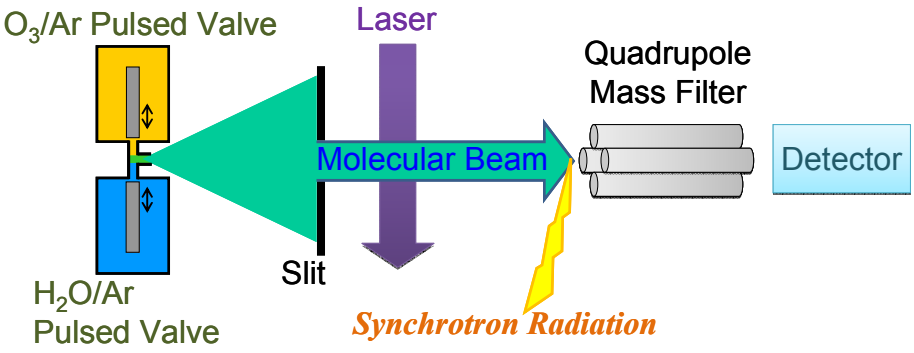

Figure S1. Experimental schematic (not to scale). The ozone/argon gas and water/argon gas, injected from two pulsed valves, were mixed in a small volume and expanded into a vacuum chamber to form a molecular beam, of which the size was confined by a slit. After interaction with a laser beam, the molecular beam was photoionized by synchrotron radiation, and the resulted ions at a desired mass-to-charge ratio (m/z) were selected by a quadrupole mass filter before reaching an ion detector.

Ozone/argon sample preparation:

Ozone was prepared by flowing O_2 (99.999%, Air Liquid, Inc.) through a commercial ozonizer and then concentrated with silica gel at a temperature of ~200 K. The color of the silica gel changed from white to dark blue after absorbing ozone. By warming up the silica gel, the absorbed ozone was transferred to a 5-liter stainless steel cylinder of which the bottom was cooled by liquid nitrogen. The ozone was purified by pumping out the residual oxygen gas. The pure ozone was mixed with argon buffer gas (0.5%, 1%, or 2% ozone, V/V) and stored in the same cylinder under a temperature of about 200 K (dry ice). At this low temperature, the lifetime of our ozone sample was more than a week. Mixing of the ozone and buffer gases was accelerated by convection which was induced by a temporary temperature gradient (apply a small amount of liquid nitrogen to the top of the cylinder for a couple of times).

Water/argon sample:

The H_2O/Ar mixture gas of a desired concentration was obtained by mixing a pure Ar flow and a humidified Ar flow. The flow rates of both gases were controlled by two mass flow controllers (Brooks 5850E). Because the gas flow consumed by the pulsed valve was too small

for a stable operation of the mass flow controllers, we vented most of the mixture gas to a pressure regulated gas line. Different water concentrations were obtained by adjusting the relative flow rates of the two gases.

Lasers:

Two excimer lasers (Lambda Physik, LPX 210i and LPF 220i) were used through out this experiment. The laser beam was focused with two cylindrical lenses to a suitable spot size. Because the cross section of ozone at 248.4 nm is much larger than those at other excimer wavelengths, the vertical spot size at 248.4 nm was set to be significantly larger than those at other wavelengths. Dielectric-coated optics (Laseroptik GmbH, IVA-248) was used to reduce the laser fluence homogeneously. The average laser power was measured by a thermopile power meter (Gentec-EO, UP25N).

Detector:

In the detector, the molecular beam was photoionized with synchrotron radiation from an undulator (period length = 9 cm, number of periods = 48). In this beamline (21A1 of the Taiwan Light Source),[1, 2] the synchrotron radiation passed through a windowless gas cell filled with Ar gas of 10 torr to absorb the photons at higher harmonic frequencies. Then, the photons at the fundamental frequency were focused to the photoionization region of the detector. The photon intensity was in the order of 10^{16} photon/sec. Although the residue high harmonic photons and broadband background light were relatively very weak, they still ionized the Ar buffer gas and the O_3 and H_2O monomers in the molecular beam.

II. Results and discussion

1. Mass spectra:

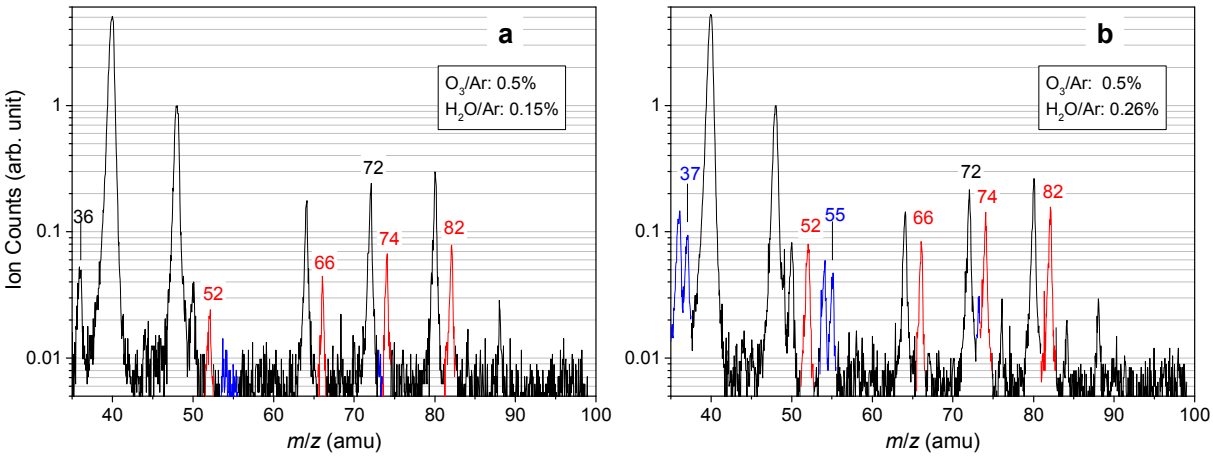

Figure S2. Photoionization mass spectra of the molecular beam at two water concentrations, (a) 0.15% and (b) 0.26%. The ionizing photon energy was 11.9 eV. The red colored peaks at m/z = 52, 66, 74 and 82 indicate ozone-water complexes; the blue colored peaks at m/z = 36, 37, 54 and 55, etc. indicate water clusters; other peaks are from monomers or other clusters. The peak at m/z = 36 also contains an isotope of Ar (0.3% abundance).

Figure S2 shows the mass spectra of our molecular beam detected with photoionization at a photon energy of 11.9 eV at two water concentrations. Dissociative ionization may take place even at this low energy, especially for hydronium ion (H_3O^+) formation which is quit exothermic. (But it takes at least two water molecules to form a hydronium ion.) At the lower water concentration (Figure S2a: water/argon 0.15%, ozone/argon 0.5%), formation of ozone-water complexes of various sizes is evidenced by the presence of mass peaks at m/z = 52 $(H_4O_3)^+$, 66 $(H_2O_4)^+$, 74 $(ArH_2O_2)^+$ and 82 $(H_2O_5)^+$. In addition, water cluster signals at m/z = 36 $(H_2O)_2^+$, 37 $(H_2O)(H_3O)^+$, 54 $(H_2O)_3^+$, 55 $(H_2O)_2(H_3O)^+$, etc. also showed up at the higher water concentration (Figure S2b: water/argon 0.26%, ozone/argon 0.5%). Notably, the peak at m/z = 66 $(O_3H_2O)^+$ may indicate the signal of the ozone-water 1:1 complex.

2. Concentration dependences:

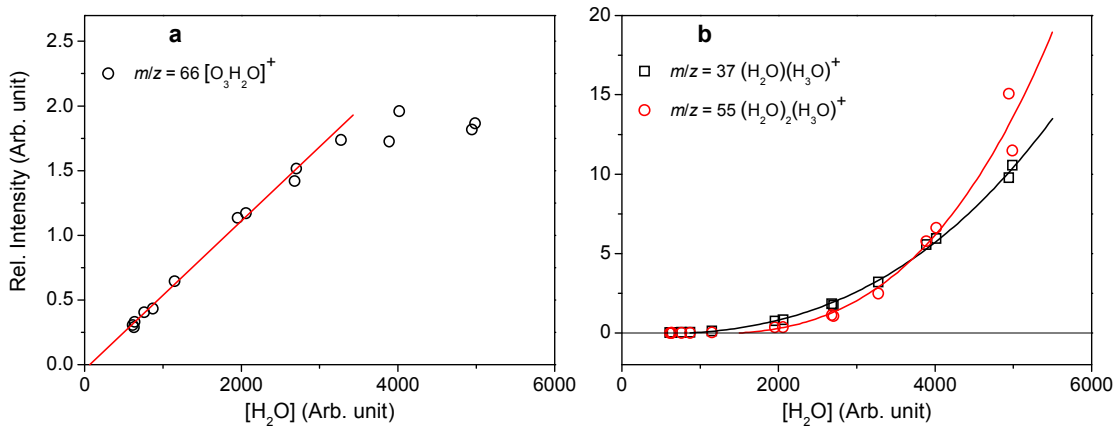

Figure S3. Comparison of the intensity variations of (a) the ozone-water complex (m/z = 66) and (b) two typical water clusters (m/z = 37, 55) as a function of the water concentration (water/argon ≤ 0.44%, recorded as the intensity of m/z = 18) in the molecular beam. The ozone concentration was 1%. Note the different y-scales.

Figure S3 shows that at low water concentrations, the intensity of m/z = 66 shows a linear rise with water concentration. This linear behavior indicates that the formation of the ozone-water complex has a first-order kinetics with respect to water concentration. Thus, the ozone-water complex may contain one water molecule in this linear region. At higher water concentrations, water clusters (e.g., m/z = 37 and 55) grow very quickly, but the intensity of the ozone-water complex (m/z = 66) shows a saturation behavior. We believe the reason is follows. Because the water-water binding[3] is much stronger than the ozone-water binding,[4-7] the water clusters compete very efficiently with the ozone-water complex (m/z = 66) at high water concentrations, such that the ozone-water complex grows much slower. This observation also suggests that the complexes with more than one water do not contribute significantly to the signal of m/z = 66.

3. Cross section ratios at 248.4 and 308.4 nm:

Table S1. Summary of the measured cross section ratios of the ozone-water complex (m/z = 66) at 248.4 and 308.4 nm. Assume ϕ = 1 for all species.

Wavelength (nm)	$[O_3]$[a]	$[H_2O]$[a]	$\frac{\sigma_{complex}}{\sigma_{O3}}$	Standard deviation[b]	Number of data points
248.4	2%	0.88%	1.07	–	3
	1%	0.88%	0.978	0.07	14
	1%	0.26%	1.01	–	3
	1%	0.26%	1.01	[c]	12
	1%	0.15%	1.13	[c]	12
	0.5%	0.88%	0.896	[c]	9
	0.5%	0.88%	0.891	[c]	7
	0.5%	0.26%	0.989	[c]	7
	0.5%	0.15%	0.950	[c]	9
308.4	0.5%	0.26%	0.98	0.075	5

[a] Volume mixing ratio in Ar buffer gas.

[b] Standard deviation of the cross section ratio.

[c] The result was obtained by using the saturation curve method (see Data analyses below).

4. Cross section at 351.8 nm:

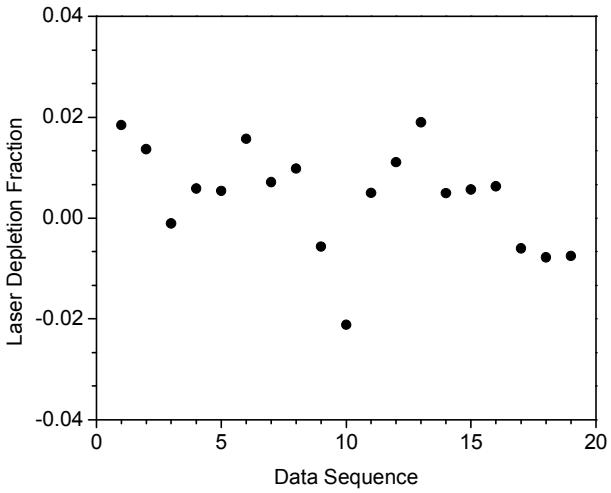

Figure S4. Laser depletion fraction of the ozone-water complex (m/z = 66) at 351.8 nm. Because no clear depletion peak could be observed at this wavelength, the laser depletion fraction was calculated by averaging the data within the time bins where the signal was expected (from the depletion peak at 248.4 nm). The results of 19 independent measurements are shown here. The average value of these data is 4.1×10^{-3} with a standard deviation of 1.03×10^{-2}. The used sample concentrations were: Data No. 1–2: $[O_3]$ = 2%; No. 3–16: $[O_3]$ = 1%; No. 17–19: $[O_3]$ = 0.5%; No. 1–7, 17: $[H_2O]$ = 0.88%; No. 8–12: $[H_2O]$ = 0.26%; No. 13–16, 18–19: $[H_2O]$ = 0.15%.

Because the average photo-depletion fraction (4.1×10^{-3}) is significantly smaller than its standard deviation (1.03×10^{-2}), we should conclude that we did not observe any photo-depletion signal of the ozone-water complex at 351.8 nm. Based on this result, we may estimate an upper limit for the depletion fraction as the sum of the average value and one standard deviation, $4.1\times10^{-3} + 1.03\times10^{-2} = 1.4\times10^{-2}$. Since the same laser fluence I could cause a depletion of 55% for Cl_2 (Figure 3C and Figure S8) which corresponds to $I\sigma = 0.79$, we deduced the upper limit of $\sigma_{complex}/\sigma_{Cl2}$ to be $1.4\times10^{-2}/0.79 = 0.018$. Taking that $\sigma_{Cl2} = 17.95\times10^{-20}$ cm^2,[8] the upper limit of $\sigma_{complex}$ is then estimated to be 0.3×10^{-20} cm^2.

III. Data analyses in detail

1. Analysis using saturation curve method:

Equation S1 describes the dependence of laser fluence for the photo-depletion process.

$$\frac{N_0 - N}{N_0} = 1 - e^{-I\sigma\phi} = 1 - e^{-I/I_0}, I_0 = \frac{1}{\sigma\phi} \qquad \text{(S1)}$$

This equation shows a saturation behavior at high laser fluences. That is, the laser-depletion signal ($N_0 - N$) will converge to N_0 at $I\sigma\phi >> 1$. Using eq. S1, fitting the photo-depletion signal as a function of laser fluence would yield the value of I_0 ($\sigma\phi = 1/I_0$). By comparing the $\sigma\phi$ value with that of a reference molecule of which the cross section is well known, we could obtain the cross section of the target species. As discussed in the main text, the dissociation yield ϕ is unity for all the studied species.

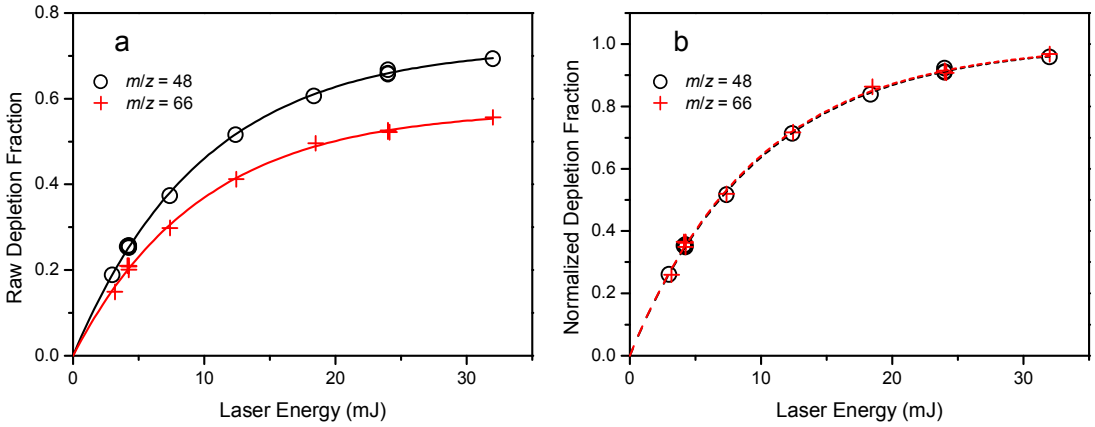

Figure S5. Photo-depletion fraction as a function of laser fluence at 248.4 nm for ozone (m/z = 48) and the ozone-water cluster (m/z = 66). Symbols: experimental data; Lines: fit with eq. S1. (a) Raw depletion fraction. (b) Normalized depletion fraction.

In Figure S5a, the laser-depletion signals show a saturation behavior which can be fit with eq. S1 very well. However, at high laser fluences, the raw depletion fractions converge to values less than unity. The reason is the following: (i) the photo-depletion signal was broadened because the molecular beam still had some velocity spread;[8] (ii) we averaged the photo-depletion

fraction in a window which covered the whole peak of the depletion signal and this average value becomes smaller as the window becomes wider. Nonetheless, as far as the choice of the average window is consistent through out the whole data set, it would not affect the cross section value at all. By fitting the laser depletion signals at m/z = 66 and 48, we found that these two species have almost the same cross sections. This becomes more obvious after we normalized the raw data with respect to their corresponding saturation values (Figure S5b) – the normalized data of m/z = 66 and 48 fully overlap. More data are shown in Figure S6 and the results are summarized in Table S1.

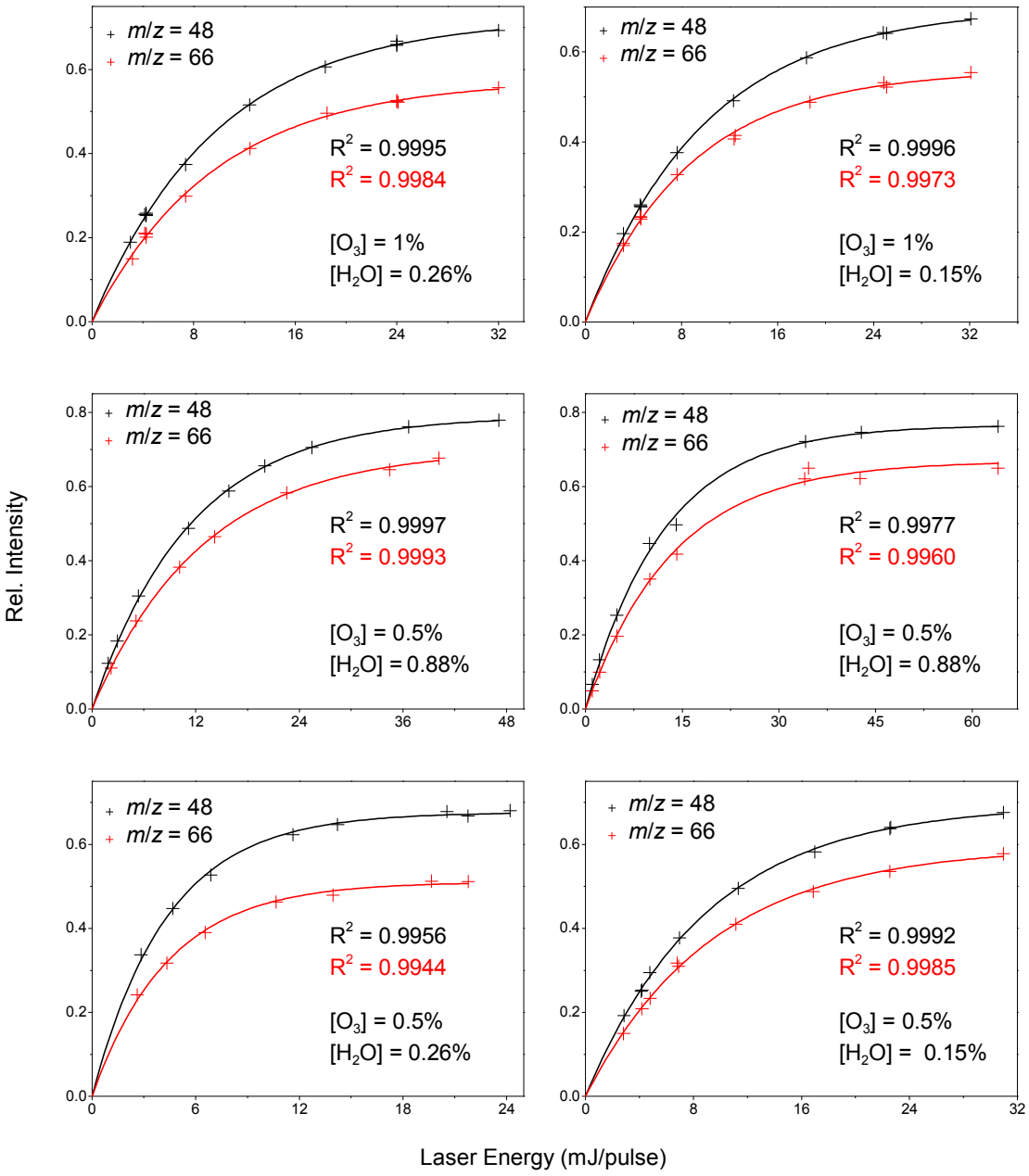

Figure S6. Saturation curves of ozone (m/z = 48) and the ozone-water cluster (m/z = 66) at different concentrations at 248.4 nm.

2. Simpler analysis for data at 248.4 and 308.4 nm:

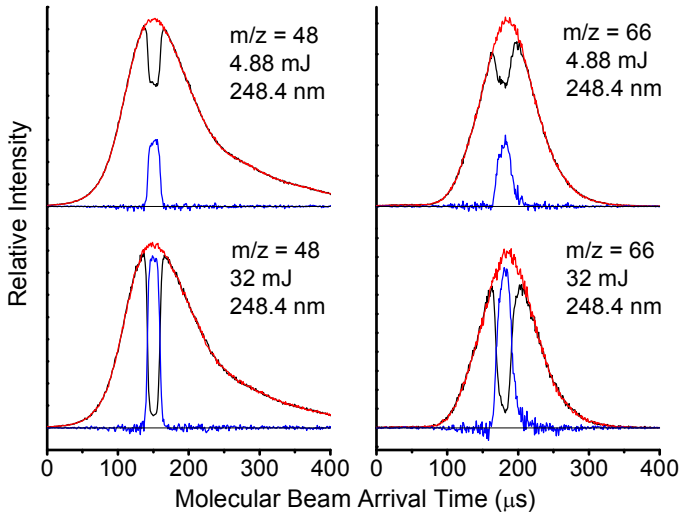

Figure S7. Normalized number-density profiles of the molecular beam showing the photo-depletion signals at two detected masses, m/z = 48 (ozone) and 66 (ozone-water cluster), at different laser fluences at 248.4 nm. Red and black lines are the detected signals before and after laser photolysis, respectively; the blue line is the photo-depletion signal.

In practice, a simpler method was also used to obtain the cross section ratio. The following equation can be deduced from eq. S1.

$$\ln(1-\frac{\Delta N}{N_0}) = -I\sigma\phi \qquad \text{(S1a)}$$

Where N_0 is the fully saturated photo-depletion signal obtained from its saturation curve and $\Delta N = N_0 - N$ is the photo-depletion signal at a low laser fluence I, as shown in the upper panels of Figure S7. If we measure N_0 and ΔN of the target and reference molecules, we could obtain its cross section ratio by using eq. S2.

$$\frac{(\sigma\phi)_{molecule}}{(\sigma\phi)_{ref}} = \frac{I_{ref}}{I_{molecule}} \times \frac{\ln(1-\frac{\Delta N}{N_0})_{molecule}}{\ln(1-\frac{\Delta N}{N_0})_{ref}} \qquad \text{(S2)}$$

In our experiment, the saturated photo-depletion signal was taken at a quite high laser

fluence, where its difference from the fully saturation limit is negligible. And the photo-depletion signal ΔN was taken at a low laser fluence corresponding to about 1/3 of the saturated photo-depletion signal. Furthermore, we repeated the measurement many times to reduce random error. By comparing with the saturation curve method, this simpler method gives similar results (see Table S1).

At 308.4 nm, because the cross section is much smaller, our laser fluence could not saturate the transition. As a result, the above method becomes useful in analyzing the data at 308.4 nm. Despite that N_0 could not be obtained directly by saturating the transition at 308.4 nm, we could use approximated N_0 obtained at 248.4 nm under a condition that both laser beams have nearly identical interaction volumes with the molecular beam. To do this, two excimer lasers (Lambda Physik LPX210i for 308.4 nm, Lambda Physik LPF 220i for 248.4 nm) were carefully aligned to overlap their laser spots. Both lasers interacted with the molecular beam alternately by switching them quickly using a beam flipper (New Focus, Model 9892). The results at 308.4 nm are listed in Table S1.

3. Analysis for data at 351.8 nm:

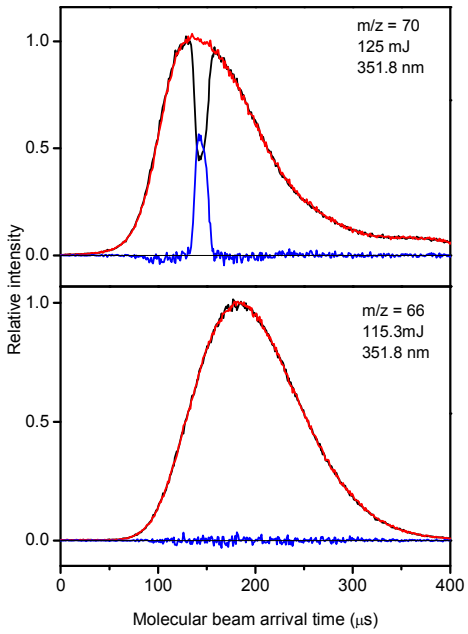

Figure S8. Normalized number-density profiles of the molecular beam showing the photo-depletion signals of two detected masses, m/z = 70 (Cl_2) and 66 (ozone-water cluster), at 351.8 nm. Black and red lines are the number of density profiles with and without laser irradiation, respectively; the blue lines are the photo-depletion signals.

Figure S8 shows there is a significant photo-depletion signal for Cl_2, but no photo-depletion signal could be observed for the ozone-water complex. We repeated the measurement for a number of times at different sample concentrations and observed similar results. To make sure the laser beam (351.8 nm) crossed the molecule beam at the peak of the intensity profile, we checked the laser delay time using the 248.4 nm laser beam. Given the significant depletion of Cl_2, we can draw a conclusion that the cross section of the ozone-water complex at 351.8 nm is very small and below our detection limit.

4. Analysis for data at 157.6 nm:

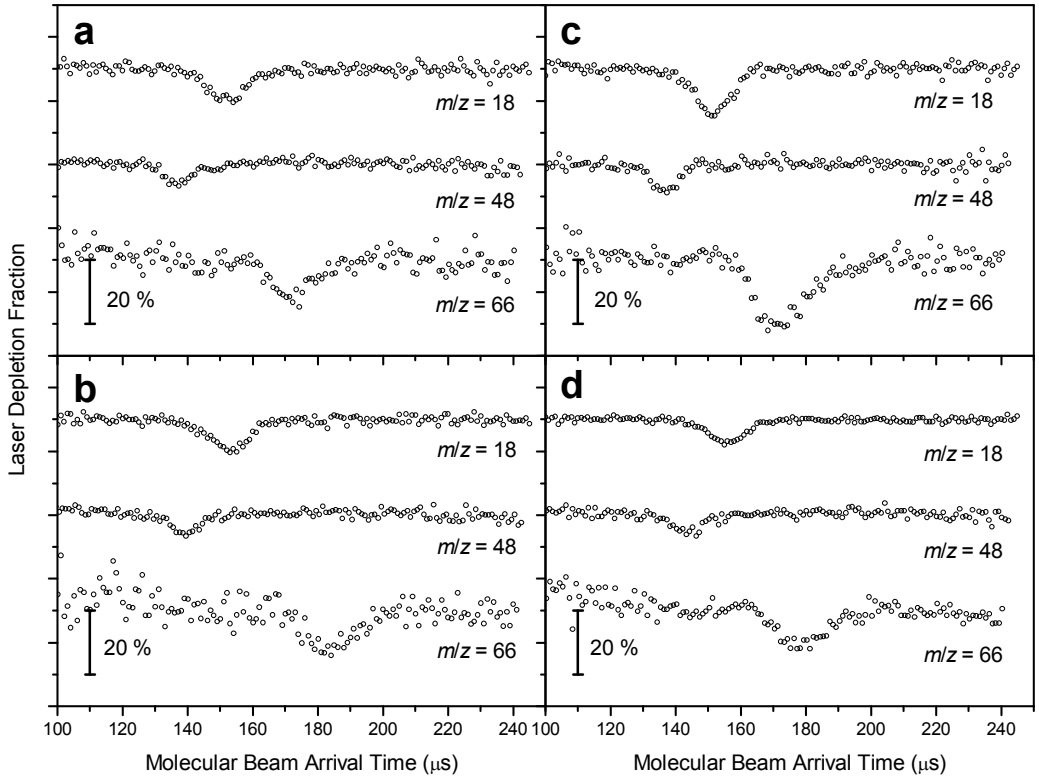

Figure S9. Photo-depletion fraction of water (m/z =18), ozone (m/z = 48) and the ozone-water complex (m/z = 66) at 157.6 nm at different water concentrations ($[O_3]$ = 1% for all). (a) $[H_2O]$ = 0.15%; (b) $[H_2O]$ = 0.17%; (c) $[H_2O]$ = 0.26%; (d) $[H_2O]$ = 0.44%. The used laser fluence was about the same within one set of experiment (one concentration condition), but different in experiments of different concentrations.

At 157.6 nm, our laser fluence could not saturate the transitions of water and ozone. Based on similar measurements (e.g., at 248.4 nm), we know that the relative error from not knowing the saturated photo-depletion signal is about 10% and less than 20%. Qualitatively the photo-depletion fraction of the ozone-water complex is about 1.5 times that of water, indicating the cross section of the complex is similar to the sum of the cross sections of ozone and water. We should note that the absolute cross sections at 157.6 nm are not the main focus of this study. More importantly, the photo-depletion fraction of the complex relative to its monomers shows no significant dependence on the water concentration (Figure S9), indicating that we were detecting a complex which contains only one water molecule.

References:

(1) Lee, S. H.; Lin, J. J.; Lee, Y. T. Selective Ionization of Photofragments Using Tunable Radiation from a Synchrotron. *J. Electron Spectrosc. Relat. Phenom.* **2005**, *144*, 135-138.

(2) Lin, J. J.; Chen, Y.; Lee, Y. Y.; Lee, Y. T.; Yang, X. M. Photodissociation Dynamics of CH_3Cl at 157.6 nm: Evidence for $CH_2(X^3B_1/a^1A_1)$+HCl Product Channels. *Chem. Phys. Lett.* **2002**, *361*, 374-382.

(3) Rocher-Casterline, B. E.; Ch'ng, L. C.; Mollner, A. K.; Reisler, H. Communication: Determination of the Bond Dissociation Energy (D_0) of the Water Dimer, $(H_2O)_2$, by Velocity Map Imaging. *J. Chem. Phys.* **2011**, *134*, 144314.

(4) Tachikawa, H.; Abe, S. Spectral Shifts of Ozone Molecule by the Complex Formation with a Water Molecule. *Chem. Phys. Lett.* **2006**, *432*, 409-413.

(5) Gillies, J. Z.; Gillies, C. W.; Suenram, R. D.; Lovas, F. J.; Schmidt, T.; Cremer, D. A Microwave Spectral and ab initio Investigation of O_3-H_2O. *J. Mol. Spectrosc.* **1991**, *146*, 493-512.

(6) Schriver, L.; Barreau, C.; Schriver, A. Infrared Spectroscopic and Photochemical Study of Water-Ozone Complexes in Solid Argon. *Chem. Phys.* **1990**, *140*, 429-438.

(7) Tsuge, M.; Tsuji, K.; Kawai, A.; Shibuya, K. Infrared Spectroscopy of Ozone-Water Complex in a Neon Matrix. *J. Phys. Chem. A* **2007**, *111*, 3540-3547.

(8) Chen, I-Cheng; Chen, Andrew F; Huang, Wen-Tsung; Takahashi, Kaito; Lin, Jim J. Photolysis Cross-Section of Ozone Dimer. *Chem.-Asian J.* **2011**, *6*, 2925.

(9) Sander, S.P.; Friedl, R. R.; Abbatt, J. P. D.; Barker, J. R.; Burkholder, J. B.; Golden, D. M.; Kolb, C. E.; Kurylo, M. J.; Moortgat, G. K.; Wine, P. H.; Huie, R. E.; Orkin, V. L. *Chemical Kinetics and Photochemical Data for Use in Atmospheric Studies 10-6*. Jet Propulsion Laboratory.